International Journal of Engineering Research & Technology (IJERT)
ISSN: 2278-0181
Vol. 15 Issue 03 , March - 2026

Freedom Analysis and Kinematic Study of a Double-Layer 3-RSR Parallel Mechanism

Xinyi Yang
(Corresponding author)
School of Mechanical Engineering
Tianjin University of Technology and Education
Tianjin 300222, China

Rui Zhang
School of Mechanical Engineering
Tianjin University of Technology and Education
Tianjin 300222, China

Minjie Cheng
School of Mechanical Engineering
Tianjin University of Technology and Education
Tianjin 300222, China

Yuhao Yang
School of Mechanical Engineering
Tianjin University of Technology and Education
Tianjin 300222, China

Yuhan Ao
School of Mechanical Engineering
Tianjin University of Technology and Education
Tianjin 300222, China

Zisun Huang
School of Mechanical Engineering
Tianjin University of Technology and Education
Tianjin 300222, China

***Abstract* - To address the limitations of traditional single-layer parallel mechanisms in terms of restricted working space and insufficient reachability, a double-layer 3-RSR parallel mechanism is proposed. This study focuses on the degree-of-freedom analysis and kinematic modeling of this mechanism. Based on screw theory, the degrees of freedom of the double-layer 3-RSR parallel mechanism are systematically analyzed, confirming it possesses three degrees of freedom: two rotational degrees of freedom around the x-axis and y-axis, and one translational degree of freedom along the z-axis. By establishing fixed and moving coordinate systems, the positive kinematic models for both single-layer and double-layer 3-RSR mechanisms were derived, yielding position and orientation parameters for the moving platform. The validity of the kinematic models was verified through joint simulation using MATLAB and SolidWorks. Results demonstrate substantial agreement between theoretical and simulated trajectories, confirming the mechanism's capability for precise control of the moving platform's path. This provides a theoretical foundation for the engineering application of double-layer 3-RSR parallel mechanisms.**

Keywords—parallel mechanism; 3-RSR; degrees of freedom; kinematic analysis; screw theory

I. INTRODUCTION

With the advancement of new industrialization and the digital transformation of traditional industries, the manufacturing sector demands higher levels of automation and precision in equipment (1). Parallel mechanisms, leveraging advantages such as high stiffness, high precision, and compact structure, have found extensive applications in precision positioning, industrial robots, and other fields (2). Compared to serial mechanisms, parallel mechanisms offer superior load-bearing capacity and motion stability, demonstrating significant application potential in complex operating conditions (3). Among these, the 3-RSR parallel mechanism, as a typical low-degree-of-freedom parallel mechanism, features a simple structure and convenient control, making it commonly used in scenarios requiring two rotary and one translational (2R1T) motions (4). However, single-layer 3-RSR mechanisms suffer from structural limitations, including restricted working space and inadequate reachability, making them ill-suited for complex tasks (5). Consequently, innovatively designing double-layer 3-RSR parallel mechanisms through stacked layering has emerged as an effective approach to expand working space and enhance reachability (6).

Degree-of-freedom analysis forms the foundation for parallel mechanism design and application, directly determining the mechanism's motion characteristics and operational range (7). Spiral theory serves as an effective tool for analyzing parallel mechanism degrees of freedom, enabling precise description of rigid body motion and constraint relationships between components (8).Numerous scholars have conducted in-depth studies on parallel mechanism degree-of-freedom analysis based on spiral theory: Wei et al. proposed a comprehensive method for non-coupled 2R1T parallel mechanisms based on branch driving force spiral theory, providing a theoretical basis for low-degree-of-freedom parallel mechanism design (9); Sun et al. employed the finite motion spiral method to describe and analyze the finite motion characteristics of 1T2R parallel mechanisms with parasitic motion (10);Fang et al. designed a 2R1T redundant-drive parallel mechanism with enhanced motion flexibility and analyzed its degrees of freedom based on spiral theory (11). These studies have advanced the development of degree-of-freedom analysis techniques for low-degree-of-freedom parallel mechanisms. However, research on degree-of-freedom analysis for double-layer stacked 3-RSR parallel mechanisms remains scarce, and the relevant theoretical framework is still incomplete (12).

Kinematics analysis constitutes a vital component of parallel mechanism research, involving the determination of position, velocity, and acceleration to provide a foundation for mechanism control and performance optimization (13). Regarding the kinematics analysis of 3-RSR parallel

Supported by the National College Students' Innovation and Entrepreneurship Training Program（Project ID: 202510066034）

International Journal of Engineering Research & Technology (IJERT)
ISSN: 2278-0181
Vol. 15 Issue 03 , March - 2026

mechanisms, scholars worldwide have achieved a series of results: Wang et al. conducted inverse kinematics and workspace analysis on the 2-RPU/UPRS mechanism, verifying its smooth motion characteristics under large-angle conditions through Adams simulation (14);Li et al. added angle sensors at the ball joints of the 3-RSR mechanism and constructed constraint equations to resolve the multiple solutions problem in forward kinematics (15); Herrero et al. optimized the 2PRU-1PRS parallel robot based on workspace and power consumption criteria and conducted in-depth kinematic analysis (16).However, the double-layer 3-RSR parallel mechanism exhibits more complex kinematic characteristics than single-layer mechanisms due to the superposition of upper and lower layers, rendering existing single-layer kinematic analysis methods inapplicable (17). Therefore, targeted research on kinematic modeling and solution for double-layer 3-RSR parallel mechanisms holds significant theoretical and engineering importance (18).

In summary, this study focuses on the degree-of-freedom analysis and kinematics research of double-layer 3-RSR parallel mechanisms. Based on screw theory, the mechanism's degrees of freedom are analyzed to clarify its motion characteristics. Positive kinematic models for both single-layer and double-layer mechanisms are established, with model validity verified through simulation. This provides theoretical support for the mechanism's design and application, holding significant engineering value for advancing the expanded application of low-degree-of-freedom parallel mechanisms (19-25).

II. SPIRAL THEORY FUNDAMENTALS

Rigid-body motion is typically categorized into finite motion and instantaneous motion. Finite rotors describe continuous motion processes, while instantaneous rotors characterize instantaneous motion states. Compared to traditional mathematical tools, FIS theory uniformly expresses rigid-body motion in a concise six-dimensional pseudo-vector form, achieving the organic integration of finite and instantaneous rotors through differential mapping.

According to Chasles' theorem, any rigid body motion between two poses can be equivalently represented as a helical motion around a fixed spatial axis—a composite motion involving rotation about the axis and translation along it. Thus, finite rigid body motion can be fully characterized by the spatial position L_f , rotation angle θ , and translation distance t of this axis. The fundamental expression for finite rotors is:

$$S_f = 2\tan\frac{\theta}{2}\begin{pmatrix} s_f \\ r_f \times s_f \end{pmatrix} + t\begin{pmatrix} 0 \\ s_f \end{pmatrix} \tag{1}$$

In this expression, the finite rotor represents the process of a rigid body undergoing a pose transformation described by S_f : rotating about the axis L_f with angular displacement θ and translating along the axis direction t . Here, s_f denotes the unit direction vector of the motion axis, while r_f corresponds to the position vector of the axis. The calculation of finite rotors is based on rotor trigonometric operations, which are inherently complex nonlinear computations. They characterize continuous rigid-body motion by integrating rotation and translation parameters to achieve precise representation of spatial pose evolution. Such operations play a pivotal role in rigid-body kinematic analysis, particularly in solving the motion of multi-degree-of-freedom parallel mechanisms.

If a rigid body undergoes two consecutive finite displacements, $S_{f,1}$ and $S_{f,2}$, these can be represented by finite rotors respectively.

$$\boldsymbol{S}_{f,1} = 2\tan\frac{\theta_1}{2}\begin{pmatrix} \boldsymbol{s}_{f,1} \\ \boldsymbol{r}_{f,1} \times \boldsymbol{s}_{f,1} \end{pmatrix} + t_1\begin{pmatrix} 0 \\ \boldsymbol{s}_{f,1} \end{pmatrix} \tag{2}$$

$$\boldsymbol{S}_{f,2} = 2\tan\frac{\theta_2}{2}\begin{pmatrix} \boldsymbol{s}_{f,2} \\ \boldsymbol{r}_{f,2} \times \boldsymbol{s}_{f,2} \end{pmatrix} + t_2\begin{pmatrix} 0 \\ \boldsymbol{s}_{f,2} \end{pmatrix} \tag{3}$$

The final continuous motion of the rigid body is then $S_{f,12}$:

$$\boldsymbol{S}_{f,12} = \boldsymbol{S}_{f,1}\Delta\boldsymbol{S}_{f,2} = \frac{\boldsymbol{s}_{f,1}+\boldsymbol{s}_{f,2}+\frac{\boldsymbol{s}_{f,2}\times\boldsymbol{s}_{f,1}}{2}-\tan\frac{\theta_1}{2}\tan\frac{\theta_2}{2}\left(t_2\begin{pmatrix}0\\ \boldsymbol{s}_{f,1}\end{pmatrix}+t_1\begin{pmatrix}0\\ \boldsymbol{s}_{f,2}\end{pmatrix}\right)}{1-\tan\frac{\theta_1}{2}\tan\frac{\theta_2}{2}\boldsymbol{s}_{f,1}^T\boldsymbol{s}_{f,2}} \tag{4}$$

where the symbol "Δ" denotes the trigonometric product operation of rotors, and "$\boldsymbol{S}_{f,2} \times S_{f,1}$ " denotes the multiplication operation of rotors.

$$\boldsymbol{S}_{f,2} \times \boldsymbol{S}_{f,1} = \begin{pmatrix} 2\tan\frac{\theta_2}{2}\boldsymbol{s}_{f,2} \times 2\tan\frac{\theta_1}{2}\boldsymbol{s}_{f,1} \\ 2\tan\frac{\theta_2}{2}\boldsymbol{s}_{f,2} \times \left(2\tan\frac{\theta_1}{2}(\boldsymbol{r}_{f,1} \times \boldsymbol{s}_{f,1}) + t_1\boldsymbol{s}_{f,1}\right) + \\ \left(2\tan\frac{\theta_2}{2}(\boldsymbol{r}_{f,2} \times \boldsymbol{s}_{f,2}) + t_1\boldsymbol{s}_{f,2}\right) \times 2\tan\frac{\theta_1}{2}\boldsymbol{s}_{f,1} \end{pmatrix} \tag{5}$$

The finite motion of a rigid body can be described as the cumulative result of multiple rotations and translations. In finite rotors, the finite motion of the nth motion joint in the nth branch can be expressed as

$$\boldsymbol{S}_{f,i,j,r} = 2\tan\frac{\theta_{i,j}}{2}\begin{pmatrix} \boldsymbol{s}_{i,j} \\ \boldsymbol{r}_{i,j} \times \boldsymbol{s}_{i,j} \end{pmatrix} \tag{6}$$

$$\boldsymbol{S}_{f,i,j,t} = t_{i,j}\begin{pmatrix} 0 \\ \boldsymbol{s}_{i,j} \end{pmatrix} \tag{7}$$

III. DEGREE OF FREEDOM ANALYSIS OF A DOUBLE-LAYER 3-RSR PARALLEL MECHANISM

A. Structure of the Double-Layer 3-RSR Parallel Mechanism

The double-layer 3-RSR parallel mechanism consists of two single-layer 3-RSR parallel mechanisms stacked vertically. It comprises a fixed platform, an intermediate platform, a moving platform, and three symmetrically distributed RSR branches. Each branch connects the fixed platform, intermediate platform, and moving platform through rotary pairs (R) and spherical joints (S) and rotary joints (R) to sequentially connect the fixed platform, intermediate platform, and moving platform. Drive joints are arranged on the fixed platform side, enabling attitude adjustment and positional movement of the moving platform

International Journal of Engineering Research & Technology (IJERT)
ISSN: 2278-0181
Vol. 15 Issue 03 , March - 2026

through branch chain transmission. The mechanism employs a layered stacking design. The upper and lower 3-RSR mechanisms achieve motion linkage through the intermediate platform. This design retains the high-precision motion characteristics of a single-stage 3-RSR mechanism while enhancing the spatial reachability of the end-effector through hierarchical coordination. Its structural properties align closely with the design requirements of the 1T2R parallel mechanism.

B. Establishment of the Screw System

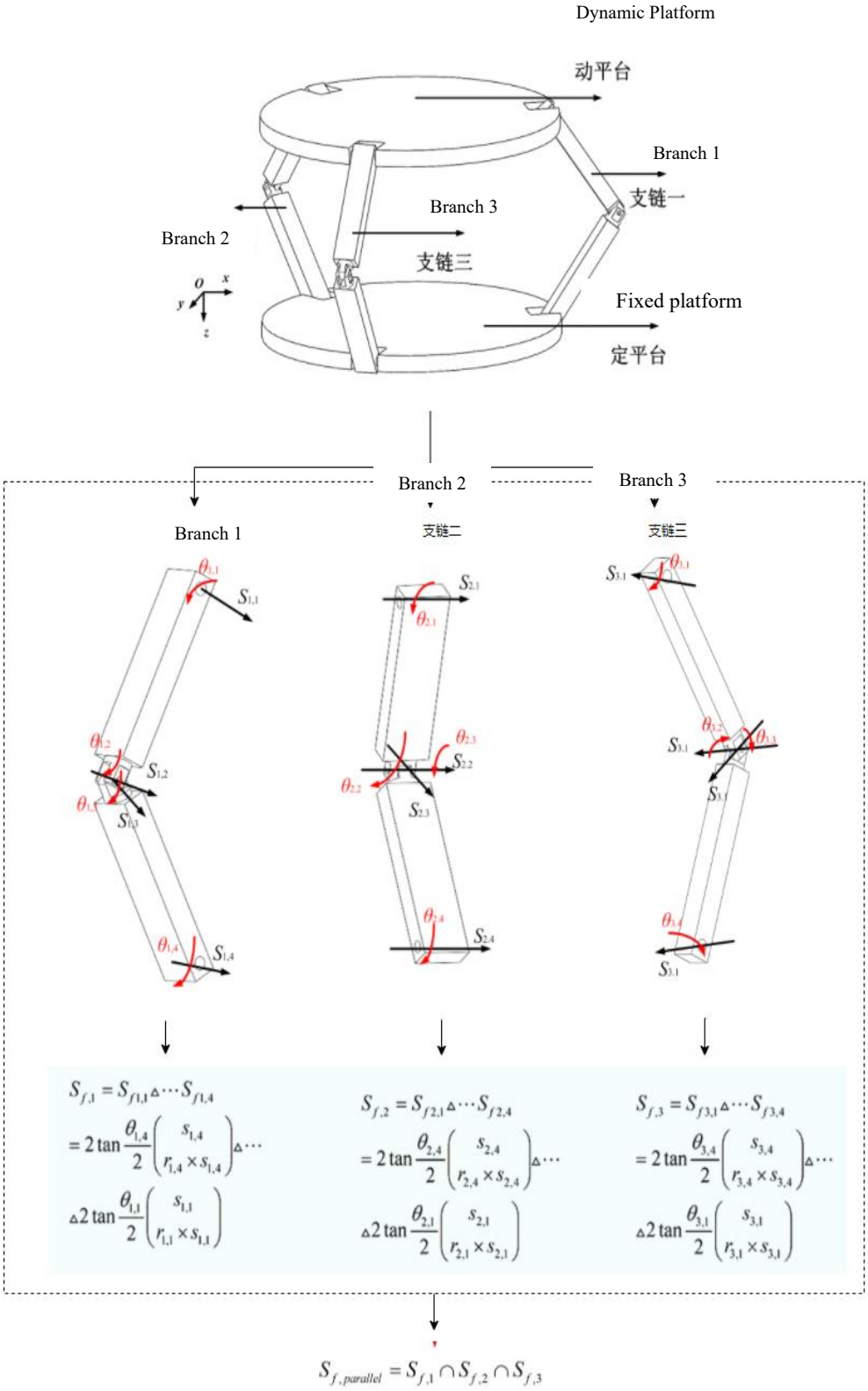

Fig. 1. Parallel Topology Mechanism

International Journal of Engineering Research & Technology (IJERT)
ISSN: 2278-0181
Vol. 15 Issue 03 , March - 2026

To analyze the degrees of freedom of the double-layer 3-RSR parallel mechanism, a branch coordinate system is first established. The origin of the branch coordinate system is selected as the center of the intermediate platform's pivot pair, where the z-axis is perpendicular to the plane of the intermediate platform and points toward the moving platform, the positive x-axis direction points toward the geometric center of the intermediate platform, and the y-axis direction is determined by the right-hand rule. Based on the mechanism's symmetry, the center of rotation (A_1、B_1、C_1) lies on the axis of the branch chain (z), and the center of rotation (D_1、Q_1) exhibits central symmetry about the origin. Consequently, the coordinate parameters of the center of rotation ($B_1(0\ \ 0\ \ a)$) and the center of rotation ($C_1(0\ \ 0\ \ -a)$、$D_1(b\ \ 0\ \ c)$、$E_1(-b\ \ 0\ \ -c)$) can be derived. According to the spatial orientation of each motion spiral in the figure, the expression for the motion spiral system of this branch chain can be constructed. The expression is:

$$\begin{cases} \$_{11}=(0\ \ 1\ \ 0\ ;\ \ 0\ \ 0\ \ 0) \\ \$_{12}=(0\ \ 1\ \ 0\ ;\ \ -a\ \ 0\ \ 0) \\ \$_{13}=(0\ \ 1\ \ 0\ ;\ \ a\ \ 0\ \ 0) \\ \$_{14}=(1\ \ 0\ \ 0\ ;\ \ 0\ \ c\ \ 0) \\ \$_{15}=(0\ \ 1\ \ 0\ ;\ \ -c\ \ 0\ \ b) \\ \$_{16}=(0\ \ 0\ \ 1\ ;\ \ 0\ \ -b\ \ 0) \\ \$_{17}=(1\ \ 0\ \ 0\ ;\ \ 0\ \ -c\ \ 0) \\ \$_{18}=(0\ \ 1\ \ 0\ ;\ \ c\ \ 0\ \ -b) \\ \$_{19}=(0\ \ 0\ \ 1\ ;\ \ 0\ \ b\ \ 0) \end{cases} \tag{8}$$

C. *Degree of Freedom Calculation*

Analysis of the RSR branch's kinematic spiral system reveals a rank of 6, indicating the branch imposes no constraints on the platform. Since the three branches are symmetrically distributed and structurally identical, the kinematic spiral system of the entire double-layer 3-RSR parallel mechanism is the intersection of the three branch systems. Thus, the moving platform possesses 6 degrees of freedom. For a single-layer 3-RSR parallel mechanism, when input conditions are specified, the motion state of the moving platform is deterministic. The moving platform, possessing 2R1T degrees of freedom, can achieve rotation and translation within a defined spatial range. For the double-layer 3-RSR parallel mechanism, the intermediate platform's link functions solely as a single-degree-of-freedom transmission component, introducing no additional degrees of freedom. Therefore, the total degrees of freedom for a double-layer 3-RSR parallel mechanism are 3: rotation about the x-axis, rotation about the y-axis, and translation along the z-axis. This degree-of-freedom configuration satisfies the "1 translation + 2 rotations" motion requirements for most precision positioning scenarios, ensuring flexible pose adjustment of the moving platform within its workspace.

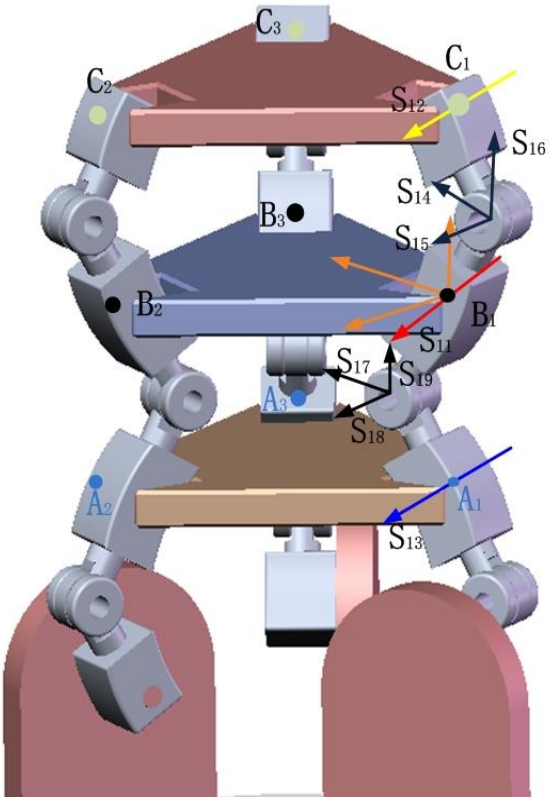

Fig. 2. Branch Coordinate System of Double-Layer 3-RSR Parallel Mechanism

International Journal of Engineering Research & Technology (IJERT)
ISSN: 2278-0181
Vol. 15 Issue 03 , March - 2026

IV. KINEMATIC ANALYSIS OF THE DOUBLE-LAYER 3-RSR PARALLEL MECHANISM

To perform kinematic analysis of the double-layer 3-RSR parallel mechanism, one must first complete the kinematic analysis of the single-layer 3-RSR mechanism and then extend it to the double-layer mechanism to determine the forward kinematic solution of the double-layer mechanism.

A. Kinematic Analysis of Single-Layer 3-RSR Mechanism

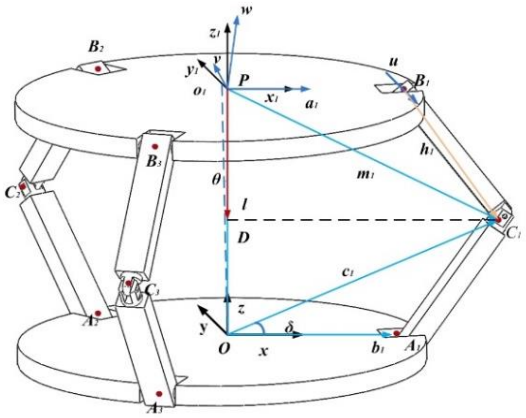

Fig. 3. Schematic Diagram of the 3-RSR Mechanism

As shown in Figure 3, establish the fixed coordinate system$O-xyz$ and the moving coordinate system$O_1-x_1y_1z_1$ on the fixed platform and moving platform, respectively. The coordinate origins$O$, O_1 are the centers of the fixed and moving platforms, respectively. The$x$ axis aligns with the vector$\boldsymbol{OA_1}$, while the$z$ axis is perpendicular to the fixed platform and points vertically upward. The x_1 axis follows the direction of vector $\boldsymbol{O_1B_1}$, z_1 The axis is perpendicular to the moving platform. Defineδ as the angle between the projection of the axis onto the base plane and the positive direction of the axis in the fixed coordinate system$x$,θ as the angle between the moving coordinate system and the axis in the fixed coordinate system$z$,l as the distance between the centers of the moving and fixed platforms,l as the angle between the axis and the z-axis of the fixed coordinate system$\varphi = \frac{\theta}{2}$, the distance from the platform center to the center of the rotating pair is$R$, and the total length of all links is$L$.

Point C_1、C_2、C_3 can be expressed using an equation containing the input angleβ_1、β_2、β_3 .

$$\boldsymbol{C}_1 = \begin{bmatrix} R - Lc\beta_1 \\ 0 \\ Ls\beta_1 \end{bmatrix} \tag{9}$$

$$\boldsymbol{C}_2 = \begin{bmatrix} -\frac{1}{2}(R - Lc\beta_2) \\ \frac{\sqrt{3}}{2}(R - Lc\beta_2) \\ Ls\beta_2 \end{bmatrix} \tag{10}$$

$$\boldsymbol{C}_3 = \begin{bmatrix} -\frac{1}{2}(R - Lc\beta_3) \\ \frac{\sqrt{3}}{2}(R - Lc\beta_2) \\ Ls\beta_3 \end{bmatrix} \tag{11}$$

Further, the vectors$\boldsymbol{C_1C_2}$ and$\boldsymbol{C_1C_3}$ are obtained as:

$$\boldsymbol{C}_1\boldsymbol{C}_2 = \begin{bmatrix} -\frac{1}{2}(3R - 2Lc\beta_1 - Lc\beta_3) \\ \frac{\sqrt{3}}{2}(R - Lc\beta_2) \\ L(s\beta_2 - s\beta_1) \end{bmatrix} \tag{12}$$

$$\boldsymbol{C}_1\boldsymbol{C}_3 = \begin{bmatrix} -\frac{1}{2}(3R - 2Lc\beta_1 - Lc\beta_3) \\ -\frac{\sqrt{3}}{2}(R - Lc\beta_3) \\ L(s\beta_3 - s\beta_1) \end{bmatrix} \tag{13}$$

Performing the cross product operation on these two vectors yields the normal vector of plane$C_1C_2C_3$, pointing from the stationary platform toward the moving platform. Using the coordinates of pointC_1 and the normal vector, we can derive the point-normal equation of plane $C_1C_2C_3$. This allows us to calculate the distance from point$O$ to plane$C_1C_2C_3$.

$$d = \frac{|-(m_1(R - Lc\beta_1) + pLs\beta_1)|}{\sqrt{{m_1}^2 + {k_1}^2 + {p_1}^2}} \tag{14}$$

The correct parameters are then:

$$l = OO_1 = 2d = \frac{2|-(m(R - Lc\beta_1) + pLs\beta_1)|}{\sqrt{m^2 + k^2 + p^2}} \tag{15}$$

$$\delta = \begin{cases} arctan\frac{k}{m} (m \geq 0, k \geq 0) \\ arctan\frac{k}{m} + \pi \quad (m < 0) \\ arctan\frac{k}{m} \quad (m \geq 0, k < 0) \end{cases} \tag{16}$$

$$\theta = 2\varphi = 2\,arctan\frac{\sqrt{m^2 + k^2}}{p} \tag{17}$$

B. Kinematic Analysis of Double-Layer 3-RSR Mechanism

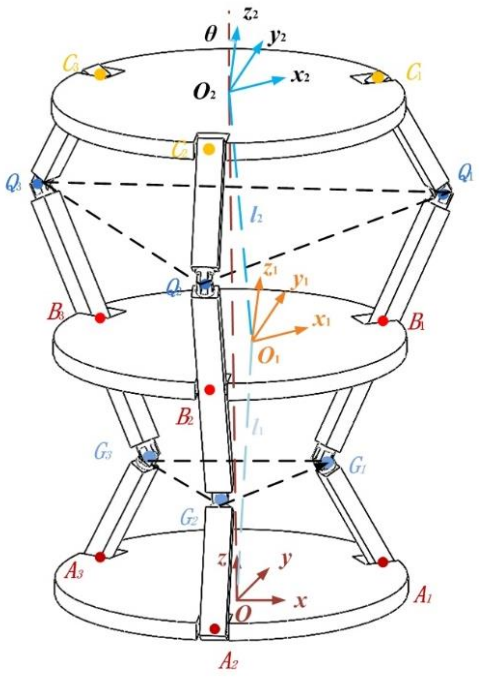

Fig. 4. Double-Layer Parallel Mechanism

International Journal of Engineering Research & Technology (IJERT)
ISSN: 2278-0181
Vol. 15 Issue 03 , March - 2026

The double-layer 3-RSR parallel mechanism can be regarded as a superposition structure of two single-layer 3-RSR parallel mechanisms. When the input angle of the lower mechanism takes a specific value, the output angle of the corresponding branch of the upper mechanism will match it. If the input angle changes, the output angle of the corresponding branch of the upper mechanism will also change according to dynamic laws. This relationship determines the motion transmission characteristics of the double-layer parallel mechanism.

As shown in Figure 4, this mechanism primarily consists of a fixed platform, a moving platform, and support links. The support links are structurally distributed uniformly in a 360-degree circular pattern. The active link connects to the moving platform at one end, responsible for transmitting motion or force inputs. The passive link connects to the stationary platform, serving to stabilize and support the structure. Through this design, the motion of the moving platform can be transmitted to the passive link via the active link, enabling precise motion control of the mechanism.

$O_2 - x_2y_2z_2$ A fixed coordinate system $O - xyz$ is established relative to the stationary platform, while a moving coordinate system $O_1 - x_1y_1z_1$ is established relative to the moving platform. The coordinate origin$O$、O_1、O_2 represents the center point of the stationary and moving platforms, respectively. The$x$ axis aligns with the direction of vector$\boldsymbol{OA}_1$, with the axis perpendicular to the stationary platform and oriented vertically upward. Thex_1 axis aligns with the direction of vector$\boldsymbol{O}_1\boldsymbol{B}_1$, with the$z_1$ axis perpendicular to the moving platform. Thex_2 axis aligns with the direction of vector$\boldsymbol{O}_2\boldsymbol{B}_2$, with the$z_2$ axis perpendicular to the moving platform. Defineδ as the angle between the projection of thez_2 axis onto the base plane and the positive direction of the$x$ axis in the moving coordinate system, ∠(m, m) as the angle between the moving coordinate system and the z_2 axis in the fixed coordinate system,l_1 as the center distance between the moving and fixed platforms,R as the distance from the platform center to the center of the rotating pair, and$L$ as the total length of all linkages. The position of point G_1、G_2、G_3 can be expressed using an equation containing the input angleβ_1、β_2、β_3.

$$\boldsymbol{G}_1 = \begin{bmatrix} R - Lc\beta_1 \\ 0 \\ Ls\beta_1 \end{bmatrix} \tag{18}$$

$$\boldsymbol{G}_2 = \begin{bmatrix} -\frac{1}{2}(R - Lc\beta_2) \\ \frac{\sqrt{3}}{2}(R - Lc\beta_2) \\ Ls\beta_2 \end{bmatrix} \tag{19}$$

$$\boldsymbol{G}_3 = \begin{bmatrix} -\frac{1}{2}(R - Lc\beta_3) \\ \frac{\sqrt{3}}{2}(R - Lc\beta_2) \\ Ls\beta_3 \end{bmatrix} \tag{20}$$

Further, vectors$\boldsymbol{G}_1\boldsymbol{G}_2$ and$\boldsymbol{G}_1\boldsymbol{G}_3$ are obtained as:

$$\boldsymbol{G}_1\boldsymbol{G}_2 = \begin{bmatrix} -\frac{1}{2}(3R - 2Lc\beta_1 - Lc\beta_2) \\ \frac{\sqrt{3}}{2}(R - Lc\beta_2) \\ L(s\beta_2 - s\beta_1) \end{bmatrix} \tag{21}$$

$$\boldsymbol{G}_1\boldsymbol{G}_3 = \begin{bmatrix} -\frac{1}{2}(3R - 2Lc\beta_1 - Lc\beta_3) \\ -\frac{\sqrt{3}}{2}(R - Lc\beta_3) \\ L(s\beta_3 - s\beta_1) \end{bmatrix} \tag{22}$$

Performing the cross product operation on these two vectors yields the normal vector of plane$G_1G_2G_3$, pointing from the stationary platform toward the moving platform. Using the coordinates of pointG_1 and this normal vector, we can derive the point-normal equation for plane $G_1G_2G_3$, enabling the calculation of the distance from point$O$ to plane$G_1G_2G_3$.

$$d = \frac{|\,-(m_1(R - Lc\beta_1) + pLs\beta_1)\,|}{\sqrt{{m_1}^2 + {k_1}^2 + {p_1}^2}} \tag{23}$$

The solution parameters are:

$$l = OO_1 = 2d = \frac{2\,|\,-(m(R - Lc\beta_1) + pLs\beta_1)\,|}{\sqrt{m^2 + k^2 + p^2}} \tag{24}$$

$$\delta = \begin{cases} arctan\dfrac{k}{m} (m \geq 0, k \geq 0) \\ arctan\dfrac{k}{m} + \pi \quad (m < 0) \\ arctan\dfrac{k}{m} \quad (m \geq 0, k < 0) \end{cases} \tag{25}$$

$$\theta = 2\varphi = 2\,arctan\frac{\sqrt{m^2 + k^2}}{p} \tag{26}$$

O_1 The rotation matrix relative to the O system can be expressed as:

$$^{O}\boldsymbol{R}_{O_1} = \begin{bmatrix} s\delta_1 v\theta_1 + c\theta_1 & -s\delta_1 c\delta_1 v\theta_1 & c\delta_1 s\theta_1 \\ -s\delta_1 c\delta_1 v\theta_1 & c^2\delta_1 v\theta_1 + c\theta_1 & s\delta_1 s\theta_1 \\ -c\delta_1 s\theta_1 & -s\delta_1 s\theta_1 & c\theta_1 \end{bmatrix} \tag{27}$$

$s\delta = sin\,\delta$, $c\theta = cos\,\theta$, $v\theta = 1 - cos\,\delta$, where$OO_2$ is the angle between the system and the fixed coordinate system$z$ axes$\varphi = \frac{\theta}{2}$

Q_1 ,Q_2 , andQ_3 relative to theO_1 coordinate system are:

$$^{O_1}\boldsymbol{Q}_1 = \begin{bmatrix} R - Lc\beta_1' \\ 0 \\ Ls\beta_1' \end{bmatrix} \tag{28}$$

$$^{O_1}\boldsymbol{Q}_2 = \begin{bmatrix} -\frac{1}{2}(R - Lc\beta_2') \\ \frac{\sqrt{3}}{2}(R - Lc\beta_2') \\ Ls\beta_2' \end{bmatrix} \tag{29}$$

$$^{O_1}\boldsymbol{Q}_3 = \begin{bmatrix} -\frac{1}{2}(R - Lc\beta_3') \\ \frac{\sqrt{3}}{2}(R - Lc\beta_3') \\ Ls\beta_3' \end{bmatrix} \tag{30}$$

Further derive the vector:

International Journal of Engineering Research & Technology (IJERT)
ISSN: 2278-0181
Vol. 15 Issue 03 , March - 2026

$$\boldsymbol{Q_1Q_2} = \begin{bmatrix} -\frac{1}{2}(3R - 2Lc\beta_1' - Lc\beta_3') \\ -\frac{\sqrt{3}}{2}(R - Lc\beta_3') \\ L(s\beta_3' - s\beta_1') \end{bmatrix} \quad (31)$$

$$\boldsymbol{Q_1Q_3} = \begin{bmatrix} -\frac{1}{2}(3R - 2Lc\beta_1' - Lc\beta_3') \\ -\frac{\sqrt{3}}{2}(R - Lc\beta_3') \\ L(s\beta_3' - s\beta_1') \end{bmatrix} \quad (32)$$

O_1 The distance to the plane$Q_1Q_2Q_3$:

$$d_2 = \frac{|\ -(m_2(R - Lc\beta_1') + p_2Ls\beta_1')\ |}{\sqrt{{m_2}^2 + {k_2}^2 + {p_2}^2}} \quad (33)$$

Therefore, the distance and solution parameters forO_1O_2 are:

$$l_2 = |O_1O_2| = 2d_2 = \frac{2\ |\ -(m_2(R - Lc\beta_1') + p_2Ls\beta_1')\ |}{\sqrt{{m_2}^2 + {k_2}^2 + {p_2}^2}} \quad (34)$$

$$\delta_2 = arctan\frac{k_2}{m_2} \quad (35)$$

$$\theta_2 = 2\,arctan\frac{\sqrt{{m_2}^2 + {k_2}^2}}{p_2} \quad (36)$$

wherem_2, p_2, k_2 are all functions of$\beta_i{}'$ and can be indirectly converted into functions ofβ_i .

The vector$\boldsymbol{OO_1}$ can be expressed as:

$$\boldsymbol{OO_1} = (l_1\,sin\,\varphi_1\,cos\,\delta_1\,, l_1\,sin\,\varphi_1\,sin\,\delta_1\,, l_1\,cos\,\varphi_1) \quad (37)$$

The vector $\boldsymbol{O_1O_2}$ can be expressed in the O_1 coordinate system as:

$${}^{O_1}\boldsymbol{O_1O_2} = (l_2\,sin\,\varphi_2\,cos\,\delta_2\,, l_2\,sin\,\varphi_2\,sin\,\delta_2\,, l_2\,cos\,\varphi_2) \quad (38)$$

The vector$\boldsymbol{OO_2}$ can be expressed as:

$$\boldsymbol{OO_2} = \boldsymbol{OO_1} + {}^{O}\boldsymbol{R}_{O_1}\boldsymbol{O_1O_2} = l_x, l_y, l_z \quad (39)$$

Center distance between moving and fixed platforms:

$$L = \sqrt{l_x^2 + l_y^2 + l_z^2} \quad (40)$$

V. NUMERICAL EXAMPLES AND SIMULATION VERIFICATION

The theoretical correctness of the designed double-layer 3-RSR parallel mechanism was verified using MATLAB and SolidWorks software.

First, the mechanism's forward kinematics were simulated and verified, with measured link lengths$L = 0.07848m$, and platform radius$r = 0.04497m$. The motion trajectory follows equations (41) to (43), as shown in Figure 5:

$$p(t) = \begin{cases} -0.8t^2 + 8t + 95 & 0 \le t \le 5 \\ 0 & 5 < t \le 15 \end{cases} \quad (41)$$

$$\theta(t) = \begin{cases} 0 & 0 \le t \le 5 \\ -0.32t^3 + 7.4t^2 - 48t + 100 & 5 < t \le 10 \\ 0 & 10 < t \le 15 \end{cases} \quad (42)$$

$$\theta(t) = \begin{cases} 0 & 0 \le t \le 5 \\ -0.32t^3 + 7.4t^2 - 48t + 100 & 5 < t \le 10 \\ 0 & 10 < t \le 15 \end{cases} \quad (43)$$

As shown in the figure 6, the theoretical trajectory calculated by MATLAB is compared with the simulated trajectory obtained from SolidWorks. The figure indicates that the two trajectories are essentially consistent, with a maximum positional error of less than 0.1 mm, verifying the correctness of the double-layer 3-RSR parallel mechanism's kinematic model. The simulation results demonstrate that this mechanism can achieve precise control of the moving platform's trajectory, meeting the requirements for precision positioning applications.

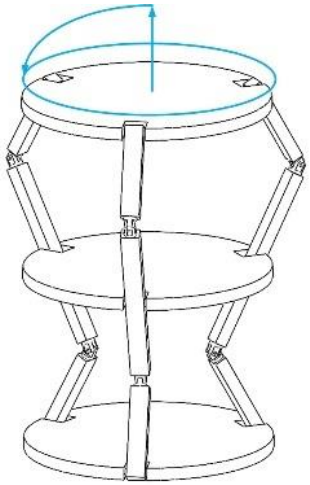

Fig. 5. Motion Trajectory of the Double-Layer Parallel Mechanism

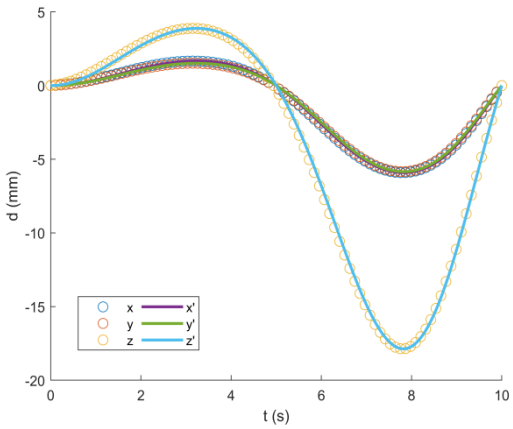

Fig. 6. Simulation of the motion position of a double-layer parallel

VI. CONCLUSIONS

This study focuses on the degree-of-freedom analysis and kinematics research of the double-layer 3-RSR parallel mechanism. The main findings are as follows:

International Journal of Engineering Research & Technology (IJERT)
ISSN: 2278-0181
Vol. 15 Issue 03 , March - 2026

(1) Based on screw theory, a motion screw system for the RSR branch of the double-layer 3-RSR parallel mechanism was established. Analysis of the mechanism's degrees of freedom confirmed it possesses three degrees of freedom: two rotational degrees of freedom about the x-axis and y-axis, and one translational degree of freedom along the z-axis. This configuration satisfies the "1 translation + 2 rotations" motion requirement.

(2) By establishing fixed, intermediate, and moving coordinate systems, the positive kinematic models for both single-layer and double-layer 3-RSR mechanisms were derived, yielding position and attitude parameters for the moving platform. The double-layer mechanism's kinematic model was constructed by superimposing the kinematic models of its upper and lower layers, accurately describing the mechanism's motion characteristics.

(3) The correctness of the kinematic models was verified through joint MATLAB and SolidWorks simulations. Theoretical trajectories closely matched simulated trajectories, with maximum positional errors below 0.1 mm. This demonstrates the mechanism's capability for precise motion platform trajectory control, providing a theoretical foundation for its engineering applications.

Future research will focus on inverse kinematics analysis and control strategy development for the double-layer 3-RSR parallel mechanism. Experimental validation using a physical prototype will further enhance mechanism performance and advance its engineering implementation.

REFERENCES

[1] Ministry of Industry and Information Technology of the People's Republic of China. Guiding Opinions on Promoting High-Quality Development of Manufacturing (Z). 2023.

[2] Ge Xin, Wang Rui, Hu Xin. Research on Improving the Quality of Primer Application in the Interior Cavities of Urban Rail Vehicles (J). Science and Technology Innovation, 2020, (24): 191-192.

[3] Hu Xin, Chen Zhuo, Wu Bo, et al. Structural Design and Automatic Spraying Process of Spray Robots for Confined Ship Cabin Spaces (J). Mechanical Design and Research, 2023, 39(04): 21-26.

[4] Peng Jun, Xue Chao, Yang Yang. Development and Application of Automatic Spraying Equipment and Coating Technology (J). Modern Coatings and Painting, 2020, 23(02): 41-43.

[5] Sun Tao, Huo X M. Synthesis of 1T2R Parallel Mechanisms with Parasitic Motion (J). Mechanical Design and Research, 2018, 128: 412-428.

[6] Fang Hailiang, Tang Taofeng, Zhang Jian. Kinematic Analysis and Comparison of 2R1T Redundant-Driven Parallel Robots and Their Non-Redundant Forms (J). Mechanical Design and Research, 2019, 142: 103587.

[7] Wei Xin, Zhang Yu, Lu Feng, et al. Topology Synthesis of Non-Coupled 2R1T Parallel Mechanisms (J). Mechanical Design, 2025, 42(01): 37-46.

[8] Zhu Xiao, Shen Hang, Li Jun, et al. Topology Design and Performance Study of a 3-DOF Parallel Mechanism with Rotatable Moving Platform (J/OL). Chinese Journal of Mechanical Engineering, 2025, (Final Accepted Manuscript).

[9] Liu Xinyu, Qi Yang. Design and Performance Analysis of a Ground-Driven Large-Part Internal Cavity Coating Mechanism (D). Tianjin: Tianjin University of Technology and Education, 2025.

[10] Huang Zhen, Li Qinchuan. Theory and Applications of Parallel Mechanisms (M). Beijing: Higher Education Press, 2021.

[11] Zhao Yong, Li Zhe. Helical Theory and Its Application in Parallel Mechanisms (J). Transactions of the Chinese Society for Mechanical Engineering, 2022, 58(11): 1-12.

[12] Wei Xin, Zhang Yu, Lu Feng, et al. Synthesis of Non-Coupled Two-Rotary-One-Translational Parallel Mechanisms (J). Mechanical Design, 2025, 42(01): 37-46.

[13] Sun Tao, Huo X M. Synthesis of 1T2R Parallel Mechanism with Parasitic Motion (J). Journal of Mechanical Design and Research, 2018, 128: 412-428.

[14] Fang Hailiang, Tang Taofeng, Zhang Jian. Kinematic Analysis and Comparison of 2R1T Redundant-Driven Parallel Robots and Their Non-Redundant Forms (J). Mechanical Design and Research, 2019, 142: 103587.

[15] Chen Yang, Guo Jun, Shen Bo, et al. Kinematic Analysis and Simulation of 3-(PRPRP)-(RS) Parallel Mechanism (J). Journal of Beihua University of Aeronautics and Astronautics, 2025, 35(02): 10-14.

[16] Li Jun, Liu Yang, Yu Zhen, et al. Design, Analysis, and Experiment of a Legged Mobile Robot (J). Journal of Applied Sciences, 2023, 13(17): 9876-9890.

[17] Wang Hao, Ma Chuang, He Yong, et al. Configuration Design and Performance Analysis of 2-RPU/UPRS Parallel Mechanism (J). Combination Machine Tools and Automated Processing Technology, 2025, (02): 40-45.

[18] Li Jun, Li Jing. Position Analysis of 3-RSR Parallel Mechanism Based on Angle Sensors (J). Manufacturing Automation, 2023, 45(03): 139-143+156.

[19] Herrero S, Pito C, Dies M, et al. Optimization of 2PRU-1PRS Parallel Robots Based on Workspace and Power Consumption Criteria (J). Journal of Applied Sciences, 2021, 11(17): 7770.

[20] Zhang B, Li Y, Wang H. Obstacle-crossing capability of a planetary wheel-legged air-ground amphibious reconnaissance robot (J). Transactions of the Chinese Society of Mechanical Engineering, 2021, 9(12): 330.

[21] Kim D, Lee S, Xu T. Foldable Hexapod Design and Field Validation for Extreme Terrain Rovers (J). IEEE Robotics and Automation Letters, 2023, 8(5): 2341-2348.

[22] Qi Yang, Qi Yue, Wu Zhe, et al. Application of an Automated Spraying System in Water-Based Coating for Railway Freight Cars (J). Railway Materials, 2023, 2(04): 55-58.

[23] Spring Systems, Inc. Electrostatic Centrifugal Spraying System (P). United States: 20230201849, 2023-06-29.

[24] Jia Xin, Guo Shuai. Design and Performance Analysis of Dual-Mode Deformable Wheels for Complex Road Surfaces (J). Journal of Tianjin University of Technology and Education, 2025, (Final Accepted Manuscript).

[25] Zhang Minghui, Shen Yiming. Study on Obstacle-Crossing Performance and Overturning Stability of Novel Leg-Deformation Mechanism (J). Journal of Mechanical Science, 2023, 14(1): 1-13.